Charge-state dependence of energy loss in random solids

B. Rosner,* S. Datz, W. Wu,† N. L. Jones, D. R. Schultz, and C. O. Reinhold
Physics Division, Oak Ridge National Laboratory, P.O. Box 2008, Oak Ridge, Tennessee 37831-6377
(Received 14 August 1997)

We measured the energy loss of 10-, 16-, and 25-MeV oxygen ions in a thin (7.5 μg/cm^2) carbon foil as a function of input charge state ($q=4-8$). At this thickness, charge-state equilibrium is nearly attained, but the energy losses accumulated over the ion's trajectory are a function of its initial charge state. Using a set of pertinent microscopic atomic collision cross sections computed using the classical trajectory Monte Carlo method, we link these parameters to the observed charge-state dependence on energy loss through a classical transport simulation. This simulation also leads to a prediction of charge-state equilibrium fractions. [S1050-2947(98)02004-6]

PACS number(s): 34.50.Bw

I. INTRODUCTION

It has been shown previously that under the conditions of ion channeling, where ion charges (q) are maintained (''frozen'') throughout their passage, the energy loss for bare ions is strictly proportional to q^2 [1,2]. For channeled ions bearing one or two electrons at ~ 2 MeV/u, the effective charge for energy loss $q_{\rm eff}$ is reduced by about 0.9 units per electron (imperfect screening) [1]. A number of studies on the effect of charge state on stopping power and effective screening by bound electrons in random solids have been carried out. These have been limited to systems in which only a few charge-changing collisions occur [3] and to cases where only two charge states are involved [4]. In these cases, the data may be adequately treated on the basis of a two-state model. Recently, Sigmund has developed expressions for the mean energy loss penetrating solids specified into entrance and exit charge states [5]. Sigmund points out that with a proper theory ''information on charge-changing cross sections, as well as the dependence of stopping power on charge state, may be gained'' and that ''to the author's (Sigmund) knowledge, no general formalism has been provided in the existing literature that would explicitly link these intercepts to pertinent atomic parameters.'' A program now exists called SRIM [6] that includes the TRIM and STOP codes. This is a useful code using principally fittings, but there is no full *ab initio* theory used [7]. In this paper, we link the pertinent atomic parameters directly to experimental data. We choose a more complex system and measure energy loss as a function of charge state and impact energy at a target thickness that gives very close to charge-state equilibrium. We then take an array of computed atomic collision cross sections (i.e., for excitation, ionization, and charge transfer) and charge-state-dependent stopping powers and, using a classical transport simulation, derive integrated energy losses as a function of input charge state and calculate the equilibrium charge distribution.

II. EXPERIMENTAL METHOD

The experiment was performed at the EN Tandem facility at Oak Ridge National Laboratory. The experimental apparatus is shown in Fig. 1. Oxygen beams with the energies of 10, 16, and 25 MeV were obtained from the EN Tandem Van de Graaff. Five charge states ranging from $q=4$ to 8 for oxygen ions were formed by stripping the high-energy negatively charged oxygen ions in a carbon foil at the high-energy terminal of the accelerator. The final ions energies and their charge states were defined by a set of two 90° analyzing and switching magnets and two sets of narrow slits beyond the magnets. The beam intensity was lowered by the two pairs of slits to a few hundred ions per second and directed toward a thin 7.5-μg/cm^2 carbon foil target positioned

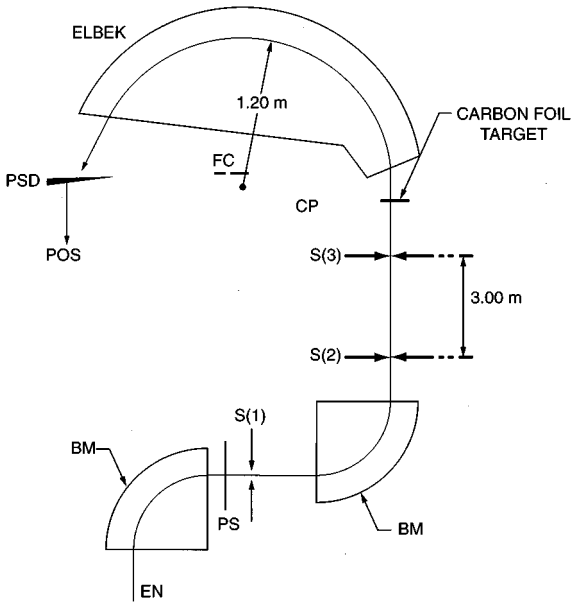

FIG. 1. Schematic diagram of the apparatus. The beam exiting the EN Tandem is analyzed by the first 90° magnet (BM) and is post stripped by a carbon foil (PS). The second BM selects the appropriate charge state. Fine energy selection is obtained by slits $S(1)$, $S(2)$, and $S(3)$ and the energy loss is measured following the Elbek magnet on a position-sensitive detector (PSD) formed from a multichannel plate.

*Present address: Department of Physics, Technion, Israel Institute of Technology, 32000 Haifa, Israel.
†Present address: Lawrence Berkeley Laboratory, 1 Cyclotron Road, MS 88, Berkeley, CA 94720.

 © 1998 The American Physical Society

TABLE I. Energy loss of O^{+q} ions in a 7.5-μg/cm^2 carbon foil as a function of their energy and entering (q_i) and exiting (q_0) charge states. The quoted errors in ΔE are based on a 1-mm position resolution. They are probably much smaller.

Energy q_i, q_0	ΔE (keV) 10 MeV	16 MeV	25 MeV
4^+	87.6±1.0	72.2±1.6	
5^+	87.5±1.0		58.9±2.5
6^+	89.8±1.0	74.2±1.6	60.8±2.5
7^+	98.2±1.0	82.6±1.6	66.7±2.5
8^+	113.8±1.0	94.2±1.6	76.9±2.5

at the entrance port of a high-resolution Elbek magnetic spectrograph [8]. The carbon foil thickness was estimated by measuring the energy loss of 2-MeV protons through it. A 20-mm position-sensitive microchannel plate (MCP) detector was mounted on the high-energy side of the focal plane of the spectrograph where its energy dispersion is the highest to determine exactly the energy of the impinging ions.

The MCP detector was calibrated by two equivalent methods. The magnetic field of the spectrograph was set so that the high-energy ion beam will hit the detector at its far end. The magnetic field was then increased a little until the beam moved to the near end of the detector. Using the well-known dispersion formula of the spectrograph, an almost linear energy calibration for the small detector was easily obtained. The calibration was confirmed by a second measurement in which the magnetic field was kept constant, by measuring the decrease in the beam energy needed to move the beam from the far end of the MCP detector to its near end.

The energy loss (ΔE) of the high-energy (E) ions in the carbon foil was determined as follows. With the carbon target in the ''out'' position, the magnetic field of the spectrograph was adjusted so that the preselected ion charge state will hit the MCP detector close to its high-energy end. From the location and the width of the beam spot on the detector,

TABLE II. Relevant mean free paths (in μg/cm^2) for oxygen ions colliding with carbon at 10, 16, and 25 MeV, computed as described in the text. The description of the reactions is given by denoting the initial and final states of the projectile ion as (q,n_1,n_2,n_3,n_4), where q is the ion charge and n_i ($i=1,2,3,4$) is the n level of each of the (up to) four electrons tracked. (For example, (4,1,1,2,2)→(5,1,1,2,0) stands for $O^{4+}(1s^2[n=2]^2 \rightarrow O^{5+}(1s^2[n=2]^1)$.) Also, numbers in brackets represent powers of 10.

Reaction	10 MeV	16 MeV	25 MeV
(4,1,1,2,2)→(5,1,1,2,0)	2.6915[−1]	3.1760[−1]	3.9387[−1]
(5,1,1,2,0)→(4,1,1,2,2)	2.6574	5.9303	1.1728[1]
(5,1,1,2,0)→(6,1,1,0,0)	8.1686[−1]	1.0497	1.2496
(5,1,1,2,0)→(6,1,2,0,0)	3.7690[1]	1.7068[1]	9.7643
(6,1,1,0,0)→(5,1,1,2,0)	1.8255	3.7622	7.4709
(6,1,2,0,0)→(5,1,1,2,0)	9.0100	4.1244	2.6574
(6,1,1,0,0)→(6,1,2,0,0)	3.0514[1]	2.7442[1]	1.8415[1]
(6,1,1,0,0)→(6,1,3,0,0)	1.8913[2]	1.1049[2]	8.9333[1]
(6,1,2,0,0)→(6,1,1,0,0)	8.3973[1]	7.8333[1]	6.3043[1]
(6,1,2,0,0)→(6,1,3,0,0)	1.5324	1.8744[1]	2.0382
(6,1,3,0,0)→(6,1,1,0,0)	8.8207[2]	1.1794[3]	7.7466[2]
(6,1,3,0,0)→(6,1,2,0,0)	3.3217	3.6766	3.9535
(6,1,1,0,0)→(7,1,0,0,0)	2.8179[1]	1.3121[1]	7.8042
(6,1,2,0,0)→(7,1,0,0,0)	8.3973[−1]	1.0291	1.3632
(6,1,3,0,0)→(7,1,0,0,0)	2.6144[−1]	3.0381[−1]	3.7826[−1]
(7,1,0,0,0)→(6,1,1,0,0)	2.8679	4.1653	9.8100
(7,1,0,0,0)→(6,1,2,0,0)	1.5904	2.7696	5.5246
(7,1,0,0,0)→(6,1,3,0,0)	3.3751	7.6063	1.6530[1]
(7,2,0,0,0)→(6,1,2,0,0)	1.4379	2.0785	4.9050
(7,3,0,0,0)→(6,1,3,0,0)	1.4379	2.0785	4.9050
(7,1,0,0,0)→(7,2,0,0,0)	4.0528[1]	3.6447[1]	3.4815[1]
(7,1,0,0,0)→(7,3,0,0,0)	2.5354[2]	1.8913[2]	1.7943[2]
(7,2,0,0,0)→(7,1,0,0,0)	5.7833[1]	4.9050[1]	4.4954[1]
(7,2,0,0,0)→(7,3,0,0,0)	2.1313	2.1035	2.6811
(7,3,0,0,0)→(7,2,0,0,0)	3.5283	3.8379	4.2844
(7,1,0,0,0)→(8,0,0,0,0)	5.7674[1]	2.6880[1]	1.7641[1]
(7,2,0,0,0)→(8,0,0,0,0)	1.0142	1.3121	1.6530
(7,3,0,0,0)→(8,0,0,0,0)	7.1895[−1]	3.7488[−1]	4.4011[−1]
(8,0,0,0,0)→(7,1,0,0,0)	1.4889	2.1400	4.2497
(8,0,0,0,0)→(7,2,0,0,0)	1.1599	1.9085	3.7622
(8,0,0,0,0)→(7,3,0,0,0)	2.3910	5.9136	1.1794[1]

the total-energy resolution of the system was determined as $\Delta E = 3 \times 10^{-4} E$. The carbon target was then lowered to its ''in'' position and the new location of the same charge-state ions on the MCP detector was determined without the need for any changes in the spectrograph magnetic field. From the difference in the position signals obtained between the out and in runs, the energy loss of the ions in the carbon foil was readily evaluated and is given in Table I.

The accuracy of the method is based on the fact that both measurements could be done without the need to change the spectrograph's field, thus avoiding any hysteresis effects. This gives, of course, an upper limit ($\sim 10\ \mu g/cm^2$) to the target thickness that can be used in the experiment. However, this is not a severe limitation even for heavier projectiles. On the other hand, such an accurate energy-loss measurement can be only done with a single outgoing charge state, the one that is identical to the incoming charge.

III. SIMULATION AND DISCUSSION

By simulating collisions of ions with foils, we can test and extend our understanding of the processes leading to the observed experimental results. For example, quantities such as the ion charge state and stopping power as a function of foil thickness can be examined. Such simulations also represent a significant challenge in that a wide range of atomic collision cross sections must be computed in order to treat the most important reactions that impinging ions suffer in their passage through the foil. These reactions determine the time-dependent charge state of the ion and therefore its accumulated energy loss.

In particular, the collision of an ion with a solid can be simulated by utilizing a classical transport approach. First, we have calculated the reaction cross sections, using the classical trajectory Monte Carlo (CTMC) method [9] as applied to binary ion-atomic collisions. The choice of this method is motivated by the fact that a wide range of reactions must be treated (i.e., state-selective charge transfer from both target K and L shells and state-selective projectile stripping for 10-, 16-, and 25-MeV O^{4-8+}+C collisions). Therefore, the theoretical method must be applicable to treating this many systems and channels quickly and reliably. The validity of the CTMC method is well established for this range of energies and collision partners, specifically, collisions involving principally one-electron processes such that $q/v \sim 1$, v being the collision velocity.

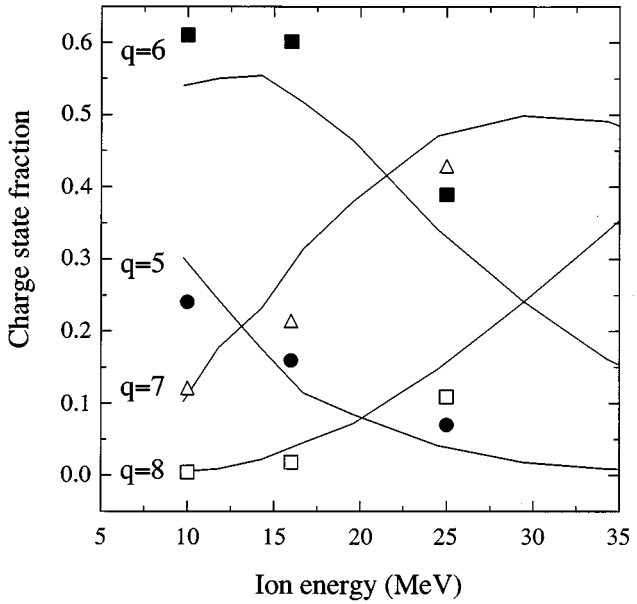

FIG. 2. Projectile charge-state fraction as a function of impacting ion energy for O^{5-8+} ions passing through thick carbon foils. The results of the present simulation are shown by symbols and the experimental results compiled by Shima, Mikumo, and Tawara [11] are shown by the curves.

The choice of reactions to include is simply based on judging which have large cross sections σ_α such that the corresponding mean free paths $\lambda_\alpha = \sigma_\alpha n$ (where n is the number density of foil atoms and α labels the reaction channel) are of the order of the foil thickness. We also neglect correlated (i.e., nonindependent) two-electron processes. Table II lists all the reactions (and their computed mean free paths) that we include. The reactions tabulated include summation over subshell contributions. Specifically, for transitions where the charge state $q \to q-1$, we include electron capture from both the L and K shells of carbon. At collision energies greater than 20 MeV capture from the K shell is dominant, but near 10 MeV, both shells' contributions are comparable. For $q \to q+1$ transitions, we include direct ionization of the projectile ion by the screened target nuclei and target electrons [10]. Since the projectile electrons in O^{5-7+} are tightly bound, the former dominates. Capture can occur into ground or excited states and collisions with target electrons and nuclei can lead to excitation rather than ionization. Projectile excitation to levels greater than $n=4$ were added to the ionization cross section since such levels would be quickly stripped by the lattice.

To calculate the stopping powers we assume that the time evolution of the charge state of the ion is a stochastic process governed by these binary collision cross sections. The probability distribution of a given reaction after a given path length x follows the Poisson distribution, i.e., $P_\alpha(x) = \lambda_\alpha^{-1} e^{x/\lambda_\alpha}$. Thus we perform a simulation in which tens of thousands of projectile trajectories are followed through steps determined by Monte Carlo sampling of the Poisson distributions for each reaction channel. Following a reaction, the next transition to occur is determined from the smallest sampled path among the open reaction channels. The resulting charge-state distributions as a function of collision energy are shown in Fig. 2 for a thick foil ($50\ \mu g/cm^2$). Our results are in good agreement with the compilation of measurements made by Shima, Mikumo, and Tawara [11]. This indicates that the atomic collision cross sections and our simulation are reasonable.

Next the energy loss ΔE of a given ion is

$$\Delta E = \sum_i f(q_i) \Delta E_H , \tag{1}$$

where the sum extends over the local values of the charge of the ion in between two charge-changing collisions. The energy loss for a given charge is extrapolated from the energy loss of protons ΔE_H in carbon foils [6] using the factors $f(q_i)$. We ignore energy straggling. The experimental en-

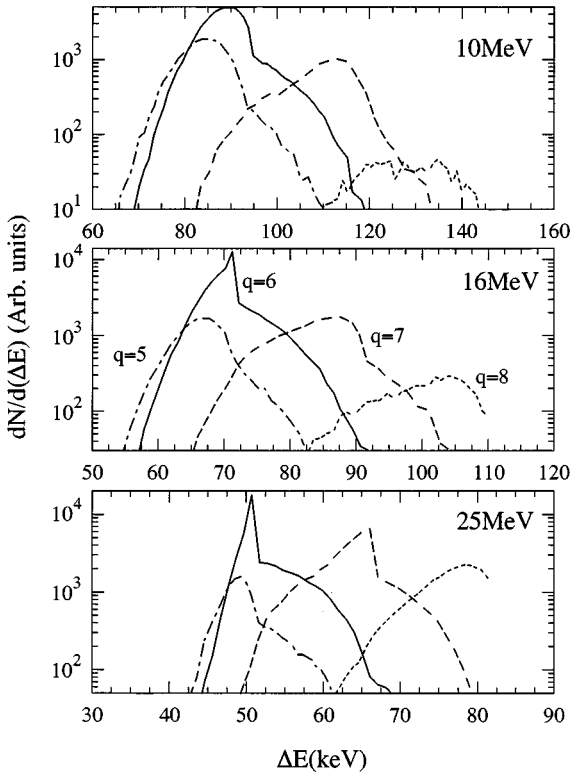

FIG. 3. Calculated differential energy-loss spectrum of 10-, 16-, and 25- O^{5-8+} ions passing through a 7.5-μg/cm^2 carbon foil. The different spectra for a given impinging energy correspond to ions that have the same exit charge as they possessed when incident on the foil.

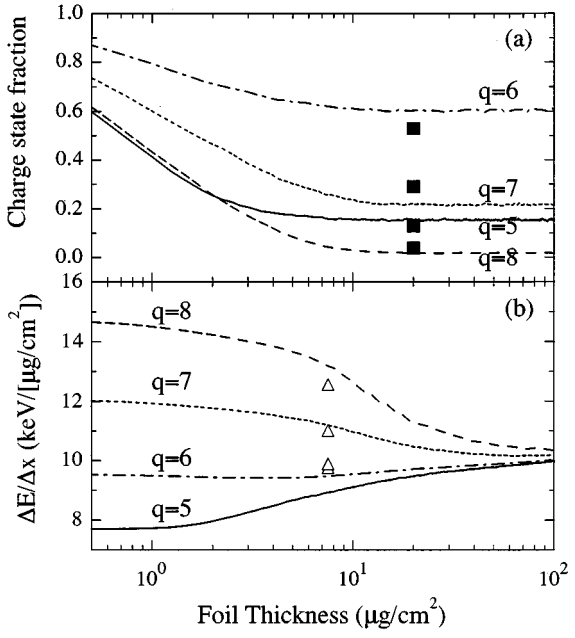

FIG. 4. (a) Charge-state fraction and (b) stopping power as a function of foil thickness for 16-MeV O^{5-8+} ions passing through carbon computed from the present simulation (curves). Also shown are the compiled charge-state fraction data of Shima, Mikumo, and Tawara [11] (solid squares) and present stopping power measurements (open triangles).

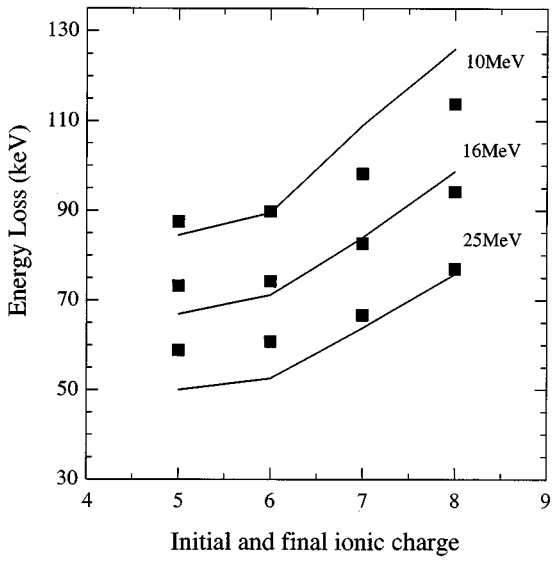

FIG. 5. Energy loss of 10-, 16-, and 25-MeV O^{5-8+} ions passing through a 7.5-μg/cm^2 carbon foil. Solid symbols indicate the present experimental results and the curves give the result of the present simulation. Note that the experiment and simulation results are determined for ions that have the same exit charge as they possessed when incident on the foil.

ergy loss corresponds to the average of ΔE over a large ensemble of ion trajectories. We estimate that even the maximum energy loss from charge-changing collisions is negligible compared to the energy loss from excitation and ionization.

For fully stripped ions, the conventional approximation (the first Born approximation) is to scale the proton-impact data by the charge squared (i.e., q^2). However, several effects modify this scaling. (i) Incomplete screening by bound electrons enhances the stopping [1,4]. That is, electrons partially screen the nuclear charge by a variable amount as a function of the distance to the nucleus, leading to enhanced ionization [12]. (ii) It is well known that this q^2 scaling breaks down for sufficiently highly charged ions (depending on v/q due to saturation). For highly charged ions the ionization probability approaches unity at small impact parameters and thus an increase of ion charge cannot lead to increased reaction probability. (iii) Finally, these effects (i) and (ii) would, in a full treatment, have to be recast into a realistic dynamic response of the solid, e.g., the full nonlinear wake, an open problem of current interest [13]. For instance, the saturation of the stopping becomes equivalent to the nonlinear response of the medium. For simplicity, in this work, we assume that the q^2 law is valid for fully stripped ions and we correct for the atomic screening by electrons in the ion by calculating the ratio of the partially stripped to fully stripping stopping in binary ion-atom collisions using the CTMC method, i.e., $f(q)=c(q)q^2$, $c(q)$ being the correction factor. $c(q)$ is of the order of 1.3 for O^{5+} and 1.06 for O^{7+}.

Thus coupling our simulation of the time-evolving charge state with the accumulation of energy loss using the appropriately scaled proton-impact stopping power data, we have obtained results for the energy losses anticipated in this ex-

periment. Figure 3 shows the calculated energy distributions of the emergent ions, illustrating the typical width due to charge-changing collisions (which is not measurable in the experiment because of the intrinsic beam width). Especially for the highest energy, the nearly discontinuous shape of the distributions near their peaks provides an indication that charge-state equilibration has not been reached.

In Fig. 4 we display the charge-state fraction and the stopping as a function of foil thickness for 16-MeV O^{q+} incidence. The upper curve shows the decay of a fixed (100%) charge state towards its equilibrium value, illustrating the thickness necessary to reach equilibrium. To this end, the cross sections have been kept constant, i.e., they do not change as the ions slow down. The charge-state fractions reach their equilibrium values for foils thicker than about $10-15\ \mu g/cm^2$. However, even though the stopping powers tend towards a common value, owing to the larger accumulated energy loss for the higher charged ions, they do not completely converge even for a very thick foil. Clearly, the present foil ($7.5\ \mu g/cm^2$) is a good candidate to observe signatures of pre-equilibrium energy loss.

Figure 5 shows the energy loss as a function of ionic charge state for various oxygen ions impinging on the thin carbon foil for three incident energies. The departure from a constant value of the stopping power reflects the fact that the foil thickness is comparable to the equilibration distances. Our calculations show that equilibration is reached after a few $\mu g/cm^2$ and therefore the rise for high-charge states is due to differences in energy loss accumulated over the path length prior to equilibration. These results can be contrasted with previous experiments at lower energies, which have shown that charge-state equilibration may be reached within one or very few atomic layers [14]. That is, in the present work the charge-transfer (filling) rates are enormously lower than those for slow collision and equilibration requires longer path lengths in the solid. The satisfactory agreement between the simulation and experiment indicates that the large quantity of atomic collision cross sections and the basic assumptions of scaled proton-carbon stopping powers are reasonable models for this case.

The agreement between theory and experiment for O^{5+} relies on the enhancement of the stopping power due to incomplete screening by bound electrons. We have also performed measurements for impinging 30-MeV Cl ions, and our calculations indicate that the incomplete atomic screening effect accounts for the significant enhancement of Cl ions over O ions of equal ionic charge. Due to the large number of electrons in Cl, we find that, for example, the experimental energy loss of Cl^{8+} is a factor of 2 larger than that for O^{8+}.

ACKNOWLEDGMENT

This research was sponsored by the U.S. Department of Energy, Office of Basic Energy Sciences, Division of Chemical Sciences, under Contract No. DE-AC05-96OR22464 with Lockheed Martin Energy Research Corporation.

[1] S. Datz, J. Gomez del Campo, P. F. Dittner, P. D. Miller, and J. A. Biggerstaff, Phys. Rev. Lett. **38**, 1145 (1977).

[2] J. A. Golovchenko, A. N. Goland, J. S. Rosner, C. E. Thorn, H. E. Wegner, H. Knudsen, and C. D. Moak, Phys. Rev. B **23**, 957 (1981).

[3] See, e.g., L. B. Bridwell, E. B. Cowen, P. M. Read, and C. J. Sofield, Nucl. Instrum. Methods Phys. Res. B **13**, 123 (1986).

[4] See, e.g., H. Ogawa, I. Katayama, Y. Sugai, M. Haruyama, K. Saito, K. Yoshida, and M. Tosaki, Nucl. Instrum. Methods Phys. Res. **115**, 66 (1996).

[5] P. Sigmund, Phys. Rev. A **50**, 3197 (1994).

[6] J. F. Ziegler, J. P. Biersack, and U. Littmark, *The Stopping and Range of Ions in Solids* (Pergamon, New York, 1985), updated in SRIM version 96.xx.

[7] G. Schiwietz (private communication).

[8] H. Schöne, S. Datz, R. Schuch, M. Schulz, P. F. Dittner, J. P. Giese, Q. C. Kessel, H. F. Krause, P. D. Miller, and C. R. Vane, Phys. Rev. A **51**, 324 (1995).

[9] R. Abrines and I. C. Percival, Proc. Phys. Soc. London **88**, 861 (1966); R. E. Olson and A. Salop, Phys. Rev. A **16**, 531 (1977).

[10] W. Lotz, Z. Phys. **216**, 241 (1968); J. J. Thomson, Philos. Mag. **23**, 449 (1912).

[11] K. Shima, T. Mikumo, and H. Tawara, At. Data Nucl. Data Tables **34**, 358 (1986).

[12] C. O. Reinhold, D. R. Schultz, and R. E. Olson, J. Phys. B **23**, L591 (1990); D. R. Schultz and R. E. Olson, *ibid.* **24**, 3409 (1991).

[13] J. M. Pitarke, A. Bergara, and R. H. Ritchie, Nucl. Instrum. Methods Phys. Res. B **99**, 187 (1995).

[14] R. Herrmann, C. L. Cocke, J. Ullrich, S. Hagmann, M. Stoekli, and H. Schmidt-Boecking, Phys. Rev. A **50**, 1435 (1994).